RSC Advances

PAPER

View Article Online
View Journal | View Issue

Cite this: *RSC Adv.*, 2024, **14**, 20145

Synthesis of Au@Ag core–shell nanocubes with finely tuned shell thicknesses for surface-enhanced Raman spectroscopic detection†

Cuixia Bi, * Xiaolong Yin and Hongyan Zhao

In this work, we describe a facile method for generating monodisperse Au@Ag core–shell nanocubes with well-controlled size and fine-tuned Ag shell thicknesses. In this synthesis method, Au nanocubes were prepared *via* the seed-mediated growth method. Then, Au@Ag nanocubes with the core–shell structure were prepared separately by reducing $AgNO_3$ with AA using as-prepared Au nanocubes as seeds. The thickness of Ag shells could be finely tuned from 3.6 nm to 10.0 nm by varying the concentration of the $AgNO_3$ precursor. By investigating the localized surface plasmon resonance (LSPR) properties of Au@Ag nanocubes in relation to the thickness of the Ag shell, we found that the intensity of the characteristic peak of Ag gradually increases and that of Au gradually decreases as the thickness of the Ag shell increases. Additionally, surface-enhanced Raman scattering (SERS) properties of Au@Ag core–shell nanocubes were evaluated using rhodamine 6G (R6G) as the probe molecule. Interestingly, Au@Ag nanocubes exhibit efficient SERS intensities compared to the Au nanocubes, and Ag shell with a thickness of about 8.4 nm exhibits the optimal SERS activity. In addition, our results also demonstrated that Au@Ag nanocubes with an Ag shell thickness of 8.4 nm exhibited high SERS sensitivity and are capable of probing the analyte down to 10^{-12} M. The results obtained here suggest that Au@Ag core–shell nanocubes might serve as a nanoprobe for SERS-based analytical and biosensing applications.

Received 27th April 2024
Accepted 12th June 2024

DOI: 10.1039/d4ra03135k

rsc.li/rsc-advances

1 Introduction

Noble metal (Au, Ag, *etc.*) nanoparticles have a strong localized surface plasmon resonance (LSPR) effect in the visible and near-infrared wavelengths, that is, free electrons on the surface of metal nanoparticles interact with external electromagnetic field to produce surface plasmon oscillation through resonance.[1–6] Due to the unique LSPR effect, metal nanoparticles exhibit excellent optical properties and thus have a wide range of applications in photonic devices, biosensing, and medical therapy.[7,8] For example, the LSPR effect can localize the light field energy to the surface of the metal structure, resulting in enhanced local electric field intensity and generating surface-enhanced Raman scattering (SERS) effect. SERS technology is a highly sensitive analysis detection tool that not only provides fingerprints of analytes but also has the characteristics of being rapid, nondestructive, less quenching and less interfering in the aqueous environment, showing great potential for applications in chemical analysis, food safety, environmental testing, and biomedicine.[9,10]

Currently, Ag nanoparticles are the best candidates for SERS substrates because of their high-intensity plasmon resonance characteristics and large-range electromagnetic field enhancement properties in the visible and near-infrared region.[11–13] However, Ag nanoparticles are thermodynamically unstable because they are susceptible to oxidation and usually prone to morphological changes, which leads to their poor durability and reproducibility in practical applications.[14] Comparatively, Au nanoparticles have excellent chemical stability, good biocompatibility and easy controllable preparation; however, the sensitivity is at least an order of magnitude lower than that of Ag nanoparticles. In this context, the bimetallic Au–Ag nanostructures are intensely studied, aiming to overcome the instability of Ag while maintaining the advantage of its excellent plasmonic response and high enhancement effect.[15–19] Specifically, growing varying thicknesses of Ag shell on Au nanoparticles to obtain bimetallic Au@Ag core–shell nanoparticles is widely considered a promising strategy to enhance chemical stability and modulate LSPR properties.[20] Such bimetallic Au@Ag core–shell nanoparticles are a type of nanotechnology that combines the properties of both Au and Ag nanomaterials. By controlling the size, shape, composition as well as the arrangement of the bimetallic Au@Ag nanoparticles, LSPR characteristics can be precisely manipulated for various applications such as sensing,[21,22] imaging,[23] catalysis,[24] bacteria detection,[25,26] and SERS.[27–29]

School of Physics and Physical Engineering, Qufu Normal University, Qufu, 273165, P. R. China. E-mail: cxbi@qfnu.edu.cn

† Electronic supplementary information (ESI) available: TEM image and UV-vis spectra of Au nanoparticles; summarized data of the Au nanocubes and Au@Ag nanocubes. See DOI: https://doi.org/10.1039/d4ra03135k

In recent years, seed-mediated growth by wet chemistry has become the most attractive technique for the preparation of bimetallic/polymetallic nanoparticles with controllable shape and size. Thanks to the efforts of many research groups, Au@Ag core–shell nanoparticles can now be prepared in many different shapes, including spheres,[30,31] cuboid,[32] cubes,[33,34] octahedral,[35] and spiky.[36] For example, Tang *et al.* synthesized Au@Ag core–shell nanocubes containing Au cores with varying shapes and sizes through modified seed-mediated methods.[20] Boubekeur-Lecaque and co-workers reported the use of DMSO for Ag growth on Au nanorod seeds allowing the formation of truncated cuboids and octahedral Au@Ag, which provides significant control over the optical response throughout the visible range.[35] This makes bimetallic Au@Ag nanoparticles a promising candidate for various applications in SERS detection, biomedical, environmental, and material science fields. Among them, Au@Ag nanocubes with a core–shell structure and cubic shape have received special attention owing to their sharp corners that are beneficial in both LSPR and SERS applications. Due to the special shape and structure of Au@Ag nanocubes, their absorption and scattering spectra have strong LSPR peaks in the visible and near-infrared spectral regions. Lin *et al.* successfully prepared a binary assembled film with diverse LSPR and SERS properties, and the near-field and far-field responses of Au nanospheres and Au@Ag core–shell nanocubes were combined by tuning and controlling the plasma coupling to improve their near-field and far-field responses.[29] In addition, the position and intensity of their LSPR peaks can be adjusted by changing the size and ratio of the core–shell structure, which can be used to realize applications such as SERS. It was proved that when the Ag shell exceeded a certain thickness, the optical properties of Au@Ag and Ag nanoparticles were similar, and Au@Ag nanoparticles with a certain Ag shell thickness exhibited better performance than that of Ag nanoparticles with the same size in the SERS application.[37]

In this study, Au@Ag core–shell nanocubes were prepared *via* a simple seed-mediated growth method (Scheme 1). The thicknesses of the Ag shell were finely tuned from 3.6 to 10.0 nm with a fixed Au core diameter. Then, we further studied the LSPR properties of the Au@Ag nanocubes as a function of the Ag shell thickness. It is worth mentioning that with the increase of Ag shell thickness, the characteristic peak intensity of Ag gradually increased, while that of Au gradually decreased. Alternatively, we evaluated the SERS properties of Au@Ag core–shell nanocubes using the R6G molecule as an analyte. Au@Ag nanocubes exhibit efficient SERS intensity compared to the Au nanocubes, and an Ag shell with a thickness of approximately 8.4 nm exhibits the optimal SERS activity. It reveals that the SERS performance is significantly enhanced by controlling Ag shell thickness. In addition, our results also demonstrate that Au@$Ag_{8.4}$ nanocubes exhibit a high SERS sensitivity and are capable of probing the analyte down to 10^{-12} M. The highly tunable LSPR, strong localized fields of the cube structures and intrinsic properties derived from the synergistic effects of Ag and Au made them particularly useful in plasmonics, SERS detection and optical sensing applications.

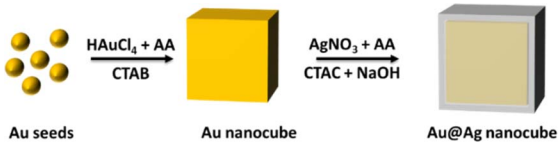

Scheme 1 Schematic illustration of the preparation process of the Au@Ag core–shell nanocubes.

2 Experimental section

2.1 Materials

Hydrogen tetrachloroaurate tetrahydrate ($HAuCl_4 \cdot 4H_2O$, 99%), cetyltrimethylammonium bromide (CTAB, 99%), cetyltrimethylammonium chloride (CTAC, 99%), sodium borohydride ($NaBH_4$, 99%), ascorbic acid (AA, 99%), sodium hydroxide (NaOH, AR) and ethanol (AR) were purchased from Sinopharm Chemical Reagent Co., Ltd (Shanghai, China). Silver nitrate ($AgNO_3$, 99+%) was purchased from Alfa Aesar (Tianjin, China). Rhodamine 6G (R6G) was purchased from Sigma-Aldrich (Beijing, China).

2.2 Synthesis of Au nanocubes

The synthesis of Au nanocubes was carried out using a seed-mediated method. The seeds solution was prepared by adding an aqueous $HAuCl_4$ solution (25 mM, 0.1 mL) into a CTAB solution (100 mM, 5 mL), then a freshly prepared, ice-cold $NaBH_4$ (10 mM, 0.6 mL) was quickly injected into the mixture under vigorous stirring for 2 min and then placed in a water bath for aging at 28 °C for 3 h. The preparation procedure for Au nanocubes was as follows. A growth solution was first prepared by mixing CTAB (100 mM, 0.9 mL) and $HAuCl_4$ (25 mM, 45 μL) in 4.5 mL H_2O. Afterward, the aqueous solution of AA (100 mM, 530 μL) was injected into the aforementioned growth solution, turning the color of the solution from yellow to colorless immediately due to Au(III) → Au(I) reduction, which was followed by the addition of the as-prepared seeds (10 μL, diluted 100 times) under vigorous stirring. After further stirring for 20 s, the resulting reaction dispersion was aged in a constant temperature water bath at 28 °C for 3 h. The obtained Au nanocubes were collected and washed with ultrapure water two times through centrifugation/redispersion cycles (at 8000 rpm and 10 min).

2.3 Preparation of Au@Ag nanocubes

All the Au@Ag nanocubes were synthesized *via* the seed-mediated method. Au@Ag nanocubes were synthesized in the CTAC solution *via* AA reduction of $AgNO_3$ onto Au nanocubes as seeds. A growth solution consisting of H_2O (4 mL), CTAC solution (100 mM, 1.0 mL), AA (100 mM, 750 μL), $AgNO_3$ solution (10 mM, 30 μL) and NaOH (1 M, 120 μL) was added to 10 mL conical flasks. Then, the seed solution of the as-prepared Au nanocubes (1 mL) was quickly injected into the above mixture under vigorous stirring. After further stirring for 5 min, the flask was transferred to a water bath at 28 °C for 12 h. The obtained Au@Ag nanocubes were collected and washed with ultrapure

water twice through centrifugation/redispersion cycles (at 6000 rpm and 10 min). The Ag shell thicknesses of the obtained Au@Ag nanocubes could be adjusted by changing the concentrations of $AgNO_3$ in the growth solutions.

2.4 Characterization

Transmission electron microscopy (TEM) images were obtained with a JEOL JEM 2100F TEM at an acceleration voltage of 200 kV. The average sizes of all the samples were obtained by statistically counting more than 100 particles based on their corresponding TEM results. UV-vis absorption spectroscopy was implemented with a Cary 50 spectrophotometer by using a 10 mm path-length quartz cuvette at room temperature.

2.5 SERS measurements

Raman spectra were recorded at room temperature using a Horiba LabRAM HR Evolution spectrograph with 633 nm as an excitation wavelength. The excitation power was 0.2 mW (0.1% of the maximum power) and the integral time was 2 s for the acquisition of one spectrum. Rhodamine 6G (R6G) was chosen as a Raman probe for the quantification of SERS enhancements. In a typical procedure, clean glass circular sheet substrates with a diameter of 6 mm were first immersed in aqua regia for 2 h, and then thoroughly rinsed with water, and the surfaces were plasma cleaned. They were placed flat on the bottom of the vessel of a 96-well plastic tissue culture plate. Subsequently, 20 μL of the prepared Au@Ag nanocubes were injected into the wells. The vessel was covered with three sheets of filter paper to reduce the rate of solvent evaporation and left to stand at 22 °C for one week until the evaporation was complete. The dried substrates were sequentially soaked in chloroform and water for 30 min to remove the free surfactant. For the SERS experiments, glass plates containing Au@Ag nanocubes were immersed into a freshly prepared 20 mL ethanol solution of R6G for 2 h. The glass substrates were then taken out and thoroughly rinsed with ethanol to remove the unbound molecule and dried with N_2 gas. The R6G concentration range used in this study was 10^{-5} to 10^{-12} M.

3 Results and discussion

3.1 Synthesis of Au nanocubes

A series of monodisperse Au nanoparticles were synthesized by varying the amount of seeds added to the growth solution. Details of the size of the Au nanoparticles obtained at different amounts of seeds and corresponding LSPR peak positions are summarized in Table S1.† As can be seen from the TEM images in Fig. 1a, when the amount of seeds added to the growth solution was 3 μL, Au nanocubes containing some irregularly shaped coproducts were obtained. The average size of the Au nanocubes was about 102 ± 7 nm. When the amount of the seeds was increased to 5 μL, the size of Au nanocubes decreased to 90 ± 5 nm and the content of the coproducts was also decreased (Fig. 1b).

As the seed volume was increased to 10 μL, the prepared Au nanocubes were homogeneous in shape and size, with good monodispersity and high yield, and no other shaped coproducts were observed (Fig. 1c). The average size of Au nanocubes was 55 ± 3 nm. Further increasing the amount of seeds to 30 μL, the size of the obtained Au nanocubes was reduced to 42 ± 3 nm (Fig. 1d). As the amount of seeds continues to increase (50 μL), the size of the product gradually decreases (38 ± 3 nm) and spherical nanoparticles appeared (Fig. 1e). When the amount of seeds was increased to 80 μL, the product changed to spherical Au nanoparticles with uniform morphology and size, and the diameter of the spherical Au nanoparticles was 35 ± 3 nm (Fig. 1f). This results indicated that the amount of seeds in the growth solution regulates the size of the final product, while it has an important influence on its morphology.

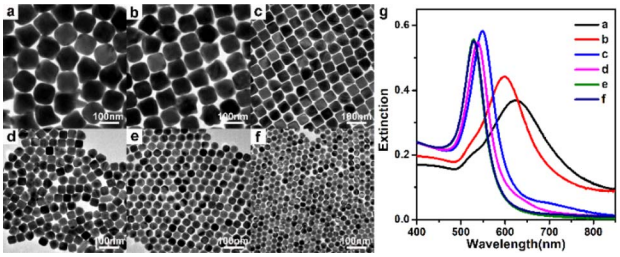

Fig. 1 TEM images (a to f) and the corresponding UV-vis absorption spectra (g) of the Au nanocubes produced at the seed volume of 3 μL, 5 μL, 10 μL, 30 μL, 50 μL, and 80 μL. The concentrations of CTAB, $HAuCl_4$, and AA in the reaction mixture are 15 mM, 0.19 mM, and 8.8 mM, respectively.

Fig. 1g shows the corresponding UV-vis absorption spectra and their absorption spectra show that the size of the products gradually decreases upon increasing the amount of seeds, and the absorption peaks gradually blue-shift from 625 nm to 598 nm, 549 nm, 537 nm, 530 nm and 529 nm (Table S1†). It is worth noting that the products in Fig. 1a and b have wider half-peak widths of the absorption spectra due to the presence of by-products. For the product corresponding to Fig. 1c, the absorption spectra of the Au nanocubes are symmetrical with narrower half-peak widths and the baseline is close to zero, which also indicates that the prepared Au nanocubes are homogeneous in shape and well monodispersed.

It is worth noting that when a very small amount of seeds was added (1 μL), irregularly shaped Au nanoparticles with branching structure were obtained, and the corresponding LSPR peak in the UV-vis spectra is located at 752 nm (Fig. S1†). When a large amount of seeds was added (150 μL), the product was spherical Au nanoparticles with a size of 30 ± 3 nm. In the UV-vis absorption spectra, the corresponding LSPR peak is located at 528 nm (Fig. S2†).

3.2 Synthesis of Au@Ag nanocubes

Au@Ag core–shell nanocubes were synthesized by reducing $AgNO_3$ with AA using the prepared 55 nm Au nanocube as the seed. The amount of Au nanocube seeds was fixed and the concentration of $AgNO_3$ was gradually increased, that is, the concentration of Ag^+ ion species was gradually increased from 15 μM to 22 μM, 29 μM, 36 μM, 44 μM, and 51 μM, to prepare

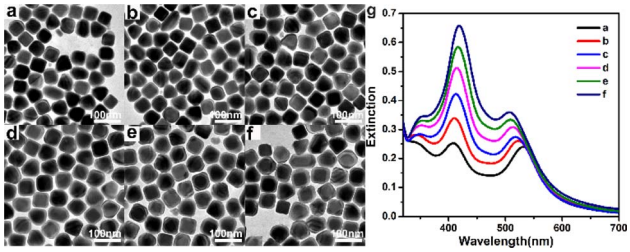

Fig. 2 TEM images (a to f) and UV-vis absorption spectra (g) of Au@Ag core–shell nanocubes with different Ag shell thicknesses obtained under different $AgNO_3$ concentrations, the $AgNO_3$ concentrations from (a) to (f) are 15 μM, 22 μM, 29 μM, 36 μM, 44 μM, and 51 μM, respectively.

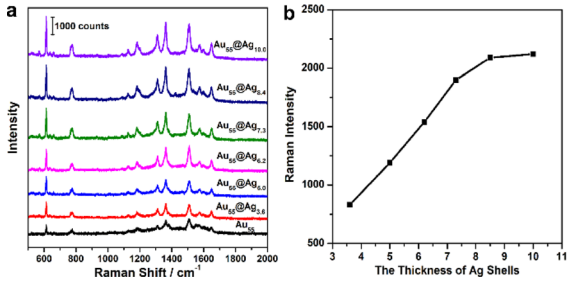

Fig. 3 (a) SERS spectra of R6G molecules (10^{-6} M) absorbed on the aggregates of corresponding 55 nm Au nanocubes, $Au_{55}@Ag_{3.6}$ nanocubes, $Au_{55}@Ag_{5.0}$ nanocubes, $Au_{55}@Ag_{6.2}$ nanocubes, $Au_{55}@Ag_{7.3}$ nanocubes, $Au_{55}@Ag_{8.4}$ nanocubes, and $Au_{55}@Ag_{10.0}$ nanocubes on glass substrates. The excitation laser wavelength for Raman measurements was 633 nm. The acquisition time was 2 s. (b) The intensities of the Raman peak at 613 cm^{-1} of the R6G molecules on aggregates of $Au_{55}@Ag_t$ NPs as a function of the thickness of Ag shells.

$Au@Ag_t$ (t is the thickness of the Ag shell) core–shell nanocubes with different Ag shell thicknesses. Details of the Ag shell thicknesses of Au@Ag core–shell nanocubes obtained under different $AgNO_3$ concentrations and corresponding LSPR peak position of Au cores and Ag shells are summarized in Table S2.† TEM images and UV-vis absorption spectra of the prepared core–shell structured Au@Ag nanocubes are shown in Fig. 2. TEM analysis and UV-vis study confirmed the formation of the core–shell nanoparticles. Because of the difference in the electron cloud density of Au and Ag atoms,[37] we were able to clearly distinguish between Au and Ag by the difference in the lining degree in the TEM photographs, thus it can be seen that our prepared Au@Ag nanocubes have a distinct core–shell structure. As shown in TEM images in Fig. 2, by controlling the addition of different amounts of $AgNO_3$ in the reaction, the Ag shell thickness of Au@Ag nanocubes gradually increased from 3.6 nm to 5.0 nm, 6.2 nm, 7.3 nm, 8.4 nm, and 10.0 nm (Table S2†), and the final product morphology remained the cube structure.

From the UV-vis absorption spectra shown in Fig. 2g, it can be seen that when the thickness of the Ag shell is 3.6 nm, the characteristic peak of Au is located at 532 nm, and the characteristic peak of Ag is located at 408 nm (Table S2†), with similar peak intensities. When the thickness of the Ag shell increases to 5.0 nm, the characteristic peaks of Au blue shift to 523 nm, the characteristic peaks of Ag red shift to 410 nm (Table S2†); and the intensity of the characteristic peaks of Ag is greater than that of the Au. With the increase of the Ag shell thickness, the characteristic peaks of Au gradually blue shift to 519 nm, 513 nm, 509 nm, and 508 nm; while the characteristic peaks of Ag gradually red shift to 412 nm, 416 nm, 417 nm, and 419 nm (Table S2†). By studying the relationship between the LSPR characteristics of Au@Ag nanocubes and the thickness of the Ag shell, it was found that the LSPR characteristic peak intensity of Ag gradually increased, while that of Au gradually decreased with the increase of the Ag shell thickness. It further indicates that the thickness of the Ag shell of the core–shell structured Au@Ag nanocubes increases with the increase of $AgNO_3$ dosage.

3.3 SERS properties of Au@Ag nanocubes

The surface-enhanced Raman properties of Au@Ag nanocubes with different Ag shell thicknesses were studied as a substrate and R6G was selected as a probe molecule. The structure has a cube shape, which can provide a large number of sharp edges and corners, facilitating their use as the SERS substrate. As shown in Fig. 3, the Raman feature peaks at 613, 775 and 1182 cm^{-1} in the SERS spectra are generated by the C–C–C intra-ring vibration mode and C–H out-of-plane bending modes and the C–H in-plane bending mode of the R6G molecule, respectively. Besides, the Raman characteristic peaks at 1310, 1362, 1510 and 1650 cm^{-1} are attributed to in-plane C–C stretching vibration modes.[38] The results indicate that Au@Ag nanocubes with different thicknesses of Ag shells showed improved SERS performances compared to Au nanocubes. Their intrinsic properties are derived from the synergistic effects of Ag and Au, thus outperforming similar nanostructures with monometallic nanoparticles.

We further explored how Ag shell thickness would affect the SERS performance of the Au@Ag nanocubes using the samples shown in Fig. 2. The SERS properties of the Au@Ag nanocubes with different thicknesses of Ag shells were evaluated by using the intensity of the characteristic peak at 613 cm^{-1} in the SERS spectra as a standard. Under the 633 nm excitation, an averaged SERS intensity out of 3 individual measurements of the same sample was 363 ± 46 photon counts for Au nanocube cores. The SERS intensity reached 830 ± 83, 1190 ± 102, 1540 ± 113, 1900 ± 125, 2090 ± 143, and 2120 ± 147 photon counts, respectively, indicating enhanced performances by 2.3, 3.3, 4.2, 5.2, 5.8, and 5.8 times for Au@Ag nanocubes with shell thickness of 3.6 nm, 5.0 nm, 6.2 nm, 7.3 nm, 8.4 nm, 10.0 nm, compared to Au nanocubes. As shown in Fig. 3b, the SERS intensity of Au@Ag nanocubes firstly increases with the thickness of the Ag shell and approaches the optimal value once the thickness of the Ag shell exceeds the critical Ag shell thickness. When the Ag shell thickness increased to 8.4 nm, the Au@Ag nanocubes basically reached the optimal SERS performance. Once the thickness of the Ag shell exceeds 8.4 nm, the surface Raman enhancement of Au@Ag nanocubes almost approaches the maximum value of the series. From the LSPR spectra, it can be seen that the

characteristic peak intensity of Ag is much stronger than that of Au after reaching this critical value of 8.4 nm. The interaction between Au and Ag is likely to be optimal at this Ag shell thickness. Therefore, we consider that after the thickness of the Ag shell of Au@Ag nanocubes reaches a critical value, its Raman enhancement property is close to the maximum value of the SERS property of Au@Ag nanocubes. The results indicate that the SERS performance is significantly enhanced by controlling the Ag shell thickness.

Additionally, the SERS enhancement factor (EF) can be calculated using the equation:[39,40] $EF = (I_{SERS} \times N_{Raman})/(I_{Raman} \times N_{SERS})$, where I_{SERS} and I_{Raman} represent the peak intensities in the SERS spectrum with 1×10^{-6} M R6G and the normal Raman spectrum with a 1×10^{-2} M R6G solution, respectively. N_{Raman} is the total number of probe molecules in the excitation volume for the normal Raman measurements and N_{SERS} is the total number of adsorbed molecules on the NPs in the SERS effective area. Fig. S3† shows the Raman spectra of 10^{-2} M R6G from the as-prepared substrates. In this experiment, we selected the intensity of the predominant peak of R6G at 613 cm^{-1} for the EF calculations. The EF of the 55 nm Au nanocubes, $Au_{55}@Ag_{3.6}$ nanocubes, $Au_{55}@Ag_{5.0}$ nanocubes, $Au_{55}@Ag_{6.2}$ nanocubes, $Au_{55}@Ag_{7.3}$ nanocubes, $Au_{55}@Ag_{8.4}$ nanocubes, and $Au_{55}@Ag_{10.0}$ nanocubes SERS substrate were evaluated to be 4.11×10^6, 9.54×10^6, 1.37×10^7, 1.77×10^7, 2.29×10^7, 2.41×10^7, and 2.44×10^7, respectively, revealing an excellent enhanced performance of the $Au@Ag_{8.4}$ nanocubes. As compared with the previous reports with respect to the Au@AuAg yolk–shell nanostructure ($EF = 3.2 \times 10^6$),[41] undulated Au@Ag triangles ($EF = 5.1 \times 10^5$),[42] Au@Ag nanoparticles ($EF = 1.02 \times 10^7$),[43] and porous Au–Ag hybrid nanoplates ($EF = 1.4 \times 10^6$),[44] the $Au@Ag_{8.4}$ nanocubes showed a higher EF.

To better determine the Raman enhancement sensitivity of the prepared Au@Ag nanocubes, the detection limit of the SERS concentration of Au@Ag nanocubes with optimal Ag shell thickness was further investigated by using R6G as the probe molecule. As shown in Fig. 4, we tested the SERS spectra of different R6G concentrations in the range of 10^{-5} to 10^{-12} M. In the corresponding SERS spectra, we can clearly observe that the Raman signal intensity gradually decreases with the decrease of the R6G concentration. Notably, the main Raman characteristic peaks at 613, 775, 1310, 1362 and 1510 cm^{-1} can still be clearly detected even when R6G is reduced to an ultra-low concentration of 10^{-12} M. Therefore, the $Au@Ag_{8.4}$ nanocubes can reach the detection limit of 10^{-12} M for R6G, further demonstrating that the Au@Ag nanocubes substrate has excellent SERS sensitivity. This work provides sufficient experimental reference and a basis for Au@Ag nanocubes as an excellent substrate for the future development of SERS.

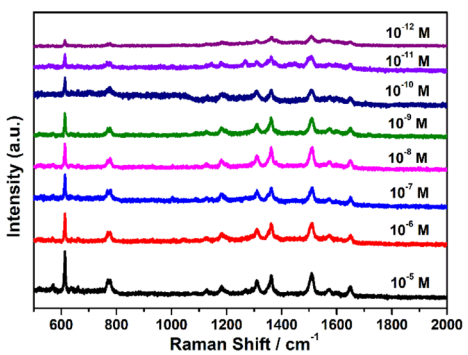

Fig. 4 Determination of SERS detection limit. Various SERS spectra of $Au@Ag_{8.4}$ nanocubes with respect to varied concentrations of R6G molecule (from 1×10^{-12} to 1×10^{-5} M).

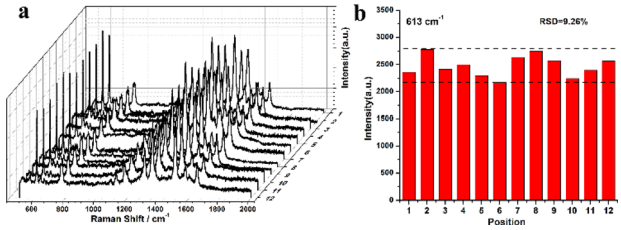

Fig. 5 Raman spectra of R6G at 1×10^{-6} M from 12 arbitrarily selected spots on the $Au@Ag_{8.4}$ nanocubes substrate (a). The histogram characterization of the intensities at the 613 cm^{-1} peak derived from Raman spectra (b).

Furthermore, the reproducibility of the SERS substrate is crucial for their practical application in molecular detection. To investigate the reproducibility and stability of the received signals for the $Au@Ag_{8.4}$ nanocubes, SERS spectra of R6G (10^{-6} M) were randomly collected at 12 different locations on three $Au@Ag_{8.4}$ nanocubes substrates (Fig. 5a). The SERS spectra from different locations exhibited similar characteristic Raman signals of R6G molecules, and the relative intensities of each peak in the spectra were the same. For any given R6G peak, there are slight intensity variations between the 12 spectra due to differences in the number of $Au@Ag_{8.4}$ nanocubes at each analysis location. The relative standard deviation (RSD) of the SERS peak intensities at 613 cm^{-1} is 9.26% (Fig. 5b). This confirms that the $Au@Ag_{8.4}$ nanocubes substrate provides excellent Raman signal reproducibility. In addition, we also used 4-ATP as a SERS probe to explore the SERS enhancement of as-prepared $Au@Ag_{8.4}$ nanocubes (Fig. S4†). It is worth noting that even when 4-ATP was reduced to an ultra-low concentration of 10^{-10} M, five well-resolved Raman signals of 4-ATP at 1078, 1141, 1392, 1437, and 1579 cm^{-1} can still be clearly detected. Therefore, the $Au@Ag_{8.4}$ nanocubes substrate has high sensitivity and good reproducibility, which provide great application potential in trace analysis.

4 Conclusion

In conclusion, we prepared monodisperse Au nanocubes with homogeneous morphology by the seed-mediated growth method. Then, Au@Ag nanocubes with core–shell structure were prepared separately by reducing $AgNO_3$ with AA using Au nanocubes as seeds. The core–shell structured Au@Ag nanocubes with tunable Ag shell thickness were obtained by adjusting the concentration of $AgNO_3$. It was found by spectral analysis that the LSPR absorption peaks of the Au core started to weaken and tended to disappear with the increase of the Ag shell thickness, while the LSPR peaks of Ag gradually enhanced,

and the LSPR peak of the Au@Ag nanocubes with the core–shell structure started to show the growth characteristics of Ag. In addition, we investigated the Raman enhancement performance of Au@Ag nanocubes with different Ag shell thicknesses on R6G separately and found that the Ag shell thickness with a size of about 8.4 nm exhibits the optimal SERS activity. It reveals that the SERS performance is significantly enhanced by controlling Ag shell thickness. In addition, our results also demonstrate that Au@Ag nanocubes with an optimized Ag shell thickness of 8.4 nm exhibit high SERS sensitivity and are capable of probing the analyte down to 10^{-12} M. Thus, Au@Ag bimetallic core–shell nanocubes are found to be suitable for efficient SERS applications.

Data availability

The data that support the findings of this study are available from the corresponding author, (Cuixia Bi), upon reasonable request.

Conflicts of interest

There are no conflicts to declare.

Acknowledgements

The authors are grateful to the financial support from the Natural Science Foundation of China (Grant no. 52101227) and Qufu Normal University for a scientific research foundation (107/613901).

References

1 M. Nasilowski, B. Mahler, E. Lhuillier, S. Ithurria and B. Dubertret, Two-Dimensional Colloidal Nanocrystals, *Chem. Rev.*, 2016, **116**(18), 10934–10982.
2 A. Ruditskiy and Y. Xia, Toward the Synthesis of Sub-15 Nm Ag Nanocubes with Sharp Corners and Edges: The Roles of Heterogeneous Nucleation and Surface Capping, *J. Am. Chem. Soc.*, 2016, **138**(9), 3161–3167.
3 S. Kessentini, D. Barchiesi, C. D'Andrea, A. Toma, N. Guillot, E. Di Fabrizio, B. Fazio, O. M. Maragó, P. G. Gucciardi and M. Lamy De La Chapelle, Gold Dimer Nanoantenna with Slanted Gap for Tunable LSPR and Improved SERS, *J. Phys. Chem. C*, 2014, **118**(6), 3209–3219.
4 M. Sun, Y. Li, B. Zhang, C. Argyropoulos, P. Sutter and E. Sutter, Plasmonic Effects on the Growth of Ag Nanocrystals in Solution, *Langmuir*, 2020, **36**(8), 2044–2051.
5 L. Lin, M. Chen, H. Qin and X. Peng, Ag Nanocrystals with Nearly Ideal Optical Quality: Synthesis, Growth Mechanism, and Characterizations, *J. Am. Chem. Soc.*, 2018, **140**(50), 17734–17742.
6 D. Hu, F. Qin, J. Liu, H. Lai, T. Tan, C. Li and C. Wang, Direction-Controlled Growth of Five-Fold Ag and Ag/Au Nanocrystals: Implications for Transparent Conductive Films, *ACS Appl. Nano Mater.*, 2022, **5**(1), 957–964.
7 M.-Q. He, S. Chen, K. Yao, J. Meng, K. Wang, Y.-L. Yu and J.-H. Wang, Precisely Tuning LSPR Property *via* "Peptide-Encoded" Morphological Evolution of Gold Nanorods for Quantitative Visualization of Enzyme Activity, *Anal. Chem.*, 2020, **92**(1), 1395–1401.
8 Z. Li, Z. Wang, J. Li, Q. Zhu, Z. Wang and Z. Dai, Enhancing Photoelectric Response of an Au@Ag/AgI Schottky Contact through Regulation of Localized Surface Plasmon Resonance, *J. Am. Chem. Soc.*, 2021, **143**(34), 13478–13482.
9 H. K. Lee, Y. H. Lee, C. S. L. Koh, G. C. Phan-Quang, X. Han, C. L. Lay, H. Y. F. Sim, Y.-C. Kao, Q. An and X. Y. Ling, Designing Surface-Enhanced Raman Scattering (SERS) Platforms beyond Hotspot Engineering: Emerging Opportunities in Analyte Manipulations and Hybrid Materials, *Chem. Soc. Rev.*, 2019, **48**(3), 731–756.
10 Z.-Y. Li, Mesoscopic and Microscopic Strategies for Engineering Plasmon-Enhanced Raman Scattering, *Adv. Opt. Mater.*, 2018, **6**(16), 1701097.
11 J. Reguera, J. Langer, D. Jiménez de Aberasturi and L. M. Liz-Marzán, Anisotropic Metal Nanoparticles for Surface Enhanced Raman Scattering, *Chem. Soc. Rev.*, 2017, **46**(13), 3866–3885.
12 X. Zhu, X. Zhuo, Q. Li, Z. Yang and J. Wang, Gold Nanobipyramid-Supported Silver Nanostructures with Narrow Plasmon Linewidths and Improved Chemical Stability, *Adv. Funct. Mater.*, 2016, **26**(3), 341–352.
13 M. Rycenga, C. M. Cobley, J. Zeng, W. Li, C. H. Moran, Q. Zhang, D. Qin and Y. Xia, Controlling the Synthesis and Assembly of Silver Nanostructures for Plasmonic Applications, *Chem. Rev.*, 2011, **111**(6), 3669–3712.
14 S. K. Krishnan, R. Esparza, F. J. Flores-Ruiz, E. Padilla-Ortega, G. Luna-Bárcenas, I. C. Sanchez and U. Pal, Seed-Mediated Growth of Ag@Au Nanodisks with Improved Chemical Stability and Surface-Enhanced Raman Scattering, *ACS Omega*, 2018, **3**(10), 12600–12608.
15 N. Cathcart, J. Chen and V. Kitaev, LSPR Tuning from 470 to 800 nm and Improved Stability of Au−Ag Nanoparticles Formed by Gold Deposition and Rebuilding in the Presence of Poly(Styrenesulfonate), *Langmuir*, 2018, **34**, 612–621.
16 V. K. Rao and T. P. Radhakrishnan, Tuning the SERS Response with Ag-Au Nanoparticle-Embedded Polymer Thin Film Substrates, *ACS Appl. Mater. Interfaces*, 2015, **7**(23), 12767–12773.
17 J. Li, Y. Zhang, S. Ding, R. Panneerselvam and T. Tian, Core−Shell Nanoparticle-Enhanced Raman Spectroscopy, *Chem. Rev.*, 2017, **117**, 5002–5069.
18 Z. Yin, Y. Wang, C. Song, L. Zheng, N. Ma, X. Liu, S. Li, L. Lin, M. Li, Y. Xu, W. Li, G. Hu, Z. Fang and D. Ma, Hybrid Au–Ag Nanostructures for Enhanced Plasmon-Driven Catalytic Selective Hydrogenation through Visible Light Irradiation and Surface-Enhanced Raman Scattering, *J. Am. Chem. Soc.*, 2018, **140**(3), 864–867.
19 Y. Yang, Q. Zhang, Z.-W. Fu and D. Qin, Transformation of Ag Nanocubes into Ag–Au Hollow Nanostructures with Enriched Ag Contents to Improve SERS Activity and

Chemical Stability, *ACS Appl. Mater. Interfaces*, 2014, **6**(5), 3750–3757.

20 J. Gong, F. Zhou, Z. Li and Z. Tang, Synthesis of Au@Ag Core–Shell Nanocubes Containing Varying Shaped Cores and Their Localized Surface Plasmon Resonances, *Langmuir*, 2012, **28**(24), 8959–8964.

21 Q. Feng, L. Qin, B. Dou, X. Han and P. Wang, Plasmon-Tunable Ag@Au Bimetallic Core−Shell Nanostructures to Enhance the Electrochemiluminescence of Quantum Dots For__MicroRNA Sensing, *ACS Appl. Nano Mater.*, 2022, **5**, 16325–16331.

22 C. Li, L. Sun, Y. Sun and T. Teranishi, One-Pot Controllable Synthesis of Au@Ag Heterogeneous Nanorods with Highly Tunable Plasmonic Absorption, *Chem. Mater.*, 2013, **25**(13), 2580–2590.

23 G. Chen, I. Roy, C. Yang and P. N. Prasad, Nanochemistry and Nanomedicine for Nanoparticle-Based Diagnostics and Therapy, *Chem. Rev.*, 2016, **116**(5), 2826–2885.

24 Y.-C. Tsao, S. Rej, C.-Y. Chiu and M. H. Huang, Aqueous Phase Synthesis of Au–Ag Core–Shell Nanocrystals with Tunable Shapes and Their Optical and Catalytic Properties, *J. Am. Chem. Soc.*, 2014, **136**(1), 396–404.

25 L. Bi, X. Wang, X. Cao, L. Liu, C. Bai, Q. Zheng, J. Choo and L. Chen, SERS-active Au@Ag core-shell nanorod (Au@AgNR) tags for ultrasensitive bacteria detection and antibiotic-susceptibility testing, *Talanta*, 2020, **220**, 121397.

26 L. Bi, H. Zhang, W. Hu, J. Chen, Y. Wu, H. Chen, B. Li, Z. Zhang, J. Jaebum Choo and L. Chen, Self-assembly of Au@AgNR along M13 framework: A SERS nanocarrier for bacterial detection and killing, *Biosens. Bioelectron.*, 2023, **237**, 115519.

27 T. Bai, J. Sun, R. Che, L. Xu, C. Yin, Z. Guo and N. Gu, Controllable Preparation of Core–Shell Au–Ag Nanoshuttles with Improved Refractive Index Sensitivity and SERS Activity, *ACS Appl. Mater. Interfaces*, 2014, **6**(5), 3331–3340.

28 J. Ma, X. Liu, R. Wang, J. Zhang, P. Jiang, Y. Wang and G. Tu, Bimetallic Core−Shell Nanostars with Tunable Surface Plasmon Resonance for Surface-Enhanced Raman Scattering, *ACS Appl. Nano Mater.*, 2020, **3**, 10885–10894.

29 S. Lin, H. Guan, Y. Liu, S. Huang, M. Li, W. Hasi, Y. Xu, J. Zou and B. Dong, Binary Plasmonic Assembly Films with Hotspot-Type-Dependent Surface-Enhanced Raman Scattering Properties, *ACS Appl. Mater. Interfaces*, 2021, **13**(44), 53289–53299.

30 K. K. Haldar, S. Kundu and A. Patra, Core-Size-Dependent Catalytic Properties of Bimetallic Au/Ag Core–Shell Nanoparticles, *ACS Appl. Mater. Interfaces*, 2014, **6**(24), 21946–21953.

31 J. Lyu, V. Geertsen, C. Hamon and D. Constantin, Determining the Morphology and Concentration of Core–Shell Au/Ag Nanoparticles, *Nanoscale Adv.*, 2020, **2**(10), 4522–4528.

32 M. Tebbe, C. Kuttner, M. Mayer, M. Maennel, N. Pazos-Perez, T. König and A. Fery, Silver-Overgrowth-Induced Changes in Intrinsic Optical Properties of Gold Nanorods: From Noninvasive Monitoring of Growth Kinetics to Tailoring Internal Mirror Charges, *J. Phys. Chem. C*, 2015, **119**, 9513–9523.

33 S. F. Tan, S. W. Chee, G. Lin, M. Bosman, M. Lin, U. Mirsaidov and C. A. Nijhuis, Real-Time Imaging of the Formation of Au–Ag Core–Shell Nanoparticles, *J. Am. Chem. Soc.*, 2016, **138**(16), 5190–5193.

34 F. Yao, J. Wang, W. Zhang, Z. Wang, Y. Li, H. Sun, Q. Chen and P. Liang, A microfluidic platform for minute-scale synthesizing Au@Ag nanocubes, *Mater. Today Chem.*, 2023, **34**, 101825.

35 I. Haidar, A. Day, P. Decorse, S. Lau-Truong, A. Chevillot-Biraud, J. Aubard, N. Félidj and L. Boubekeur-Lecaque, Tailoring the Shape of Anisotropic Core–Shell Au–Ag Nanoparticles in Dimethyl Sulfoxide, *Chem. Mater.*, 2019, **31**(8), 2741–2749.

36 Z. Huang, G. Meng, X. Hu, Q. Pan, D. Huo, H. Zhou, Y. Ke and N. Wu, Plasmon-Tunable Au@Ag Core-Shell Spiky Nanoparticles for Surface-Enhanced Raman Scattering, *Nano Res.*, 2019, **12**(2), 449–455.

37 A. K. Samal, L. Polavarapu, S. Rodal-Cedeira, L. M. Liz-Marzán, J. Pérez-Juste and I. Pastoriza-Santos, Size Tunable Au@Ag Core–Shell Nanoparticles: Synthesis and Surface-Enhanced Raman Scattering Properties, *Langmuir*, 2013, **29**(48), 15076–15082.

38 A. N. Severyukhina, B. V. Parakhonskiy, E. S. Prikhozhdenko, D. A. Gorin, G. B. Sukhorukov, H. Möhwald and A. M. Yashchenok, Nanoplasmonic Chitosan Nanofibers as Effective SERS Substrate for Detection of Small Molecules, *ACS Appl. Mater. Interfaces*, 2015, **7**(28), 15466–15473.

39 E. C. Le Ru, E. Blackie, M. Meyer and P. G. Etchegoin, Surface enhanced Raman scattering enhancement factors: a comprehensive study, *J. Phys. Chem. C*, 2007, **111**, 13794–13803.

40 H. C. Wu, T. C. Chen, H. J. Tsai and C. S. Chen, Au nanoparticles deposited on magnetic carbon nanofibers as the ultrahigh sensitive substrate for surface-enhanced Raman scattering: Detections of rhodamine 6G and aromatic amino acids, *Langmuir*, 2018, **34**(47), 14158–14168.

41 F. Zhang, N. Wu, J. Zhu, J. Zhao, G. Weng, J. Li and J. Zhao, Au@AuAg Yolk-Shell Triangular Nanoplates with Controlled Interior Gap for the Improved Surface-Enhanced Raman Scattering of Rhodamine 6G, *Sens. Actuators, B*, 2018, **271**, 174–182.

42 F. Liebig, R. M. Sarhan, C. Prietzel, C. N. Z. Schmitt, M. Bargheer and J. Koetz, Tuned Surface-Enhanced Raman Scattering Performance of Undulated Au@Ag Triangles, *ACS Appl. Nano Mater.*, 2018, **1**(4), 1995–2003.

43 K. Yuan, J. Zheng, D. Yang, B. J. Sanchez, X. Liu, X. Guo, C. Liu, N. E. Dina, J. Jian, Z. Bao, Z. Hu, Z. Liang, H. Zhou and Z. Jiang, Self-assembly of Au@ Ag nanoparticles on mussel shell to form large-scale 3D supercrystals as natural SERS substrates for the detection of pathogenic bacteria, *ACS Omega*, 2018, **3**, 2855–2864.

44 X. Wei, Q. Fan, H. Liu, Y. Bai, L. Zhang, H. Zheng, Y. Yin and C. Gao, Holey Au–Ag alloy nanoplates with built-in hotspots for surface-enhanced Raman scattering, *Nanoscale*, 2016, **8**, 15689–15695.